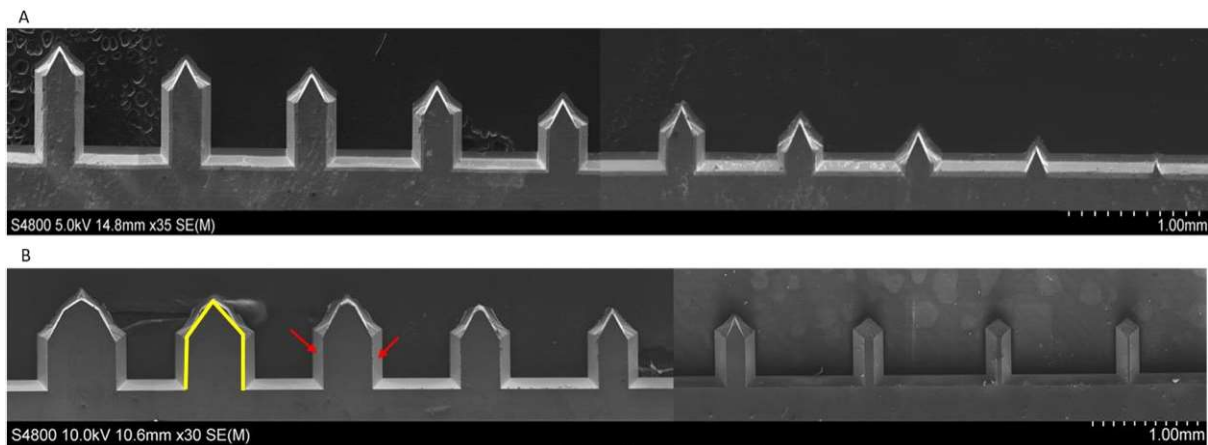


Graphical abstract:



Highlights:

- Fabrication of silicon in-plane microneedle arrays from a simple single wet etch step
- Novel microneedle design with characteristic 54.7° sidewall etch angle obtained by wet etching
- Method allows fabrication of solid microneedles with different geometries
- The microneedle arrays effectively penetrate the skin without significant indentation
- Simple, scalable and cost effective method utilises KOH to etch the silicon wafer
- Microneedle arrays demonstrate effective delivery of insulin and hyaluronic acid into skin

1
2
3
4
5
6
7
8
9

Design, fabrication, and characterisation of a silicon microneedle array for transdermal therapeutic delivery using a single step wet etch process.

10
11
12
13
14
15
16
17
18
19
20
21
22
23

Olivia Howells^a, Gareth J. Blayney^a, Benedetta Gualeni^b, James C. Birchall^b, Pey F. Eng^c, Huma Ashraf^d,
Sanjiv Sharma^{a*}, Owen J. Guy^{a*}

24
25
26
27
28
29
30
31
32
33
34
35
36
37
38
39
40
41
42
43
44
45
46
47
48
49
50
51
52
53
54
55
56
57
58
59
60
61
62
63
64
65

a. *Faculty of Science and Engineering, Swansea University, Swansea, SA1 8AE*

b. *School of Pharmacy and Pharmaceutical Sciences, Cardiff University, Cardiff, CF10 3NB*

c. *BioMEMS Technologies, Cardiff, UK*

d. *SPTS Technologies, Ringland Way, Newport, NP18 2TA, UK*

*To whom correspondence should be addressed

*College of Engineering, Fabian Way, Crymlyn Burrows, Bay Campus, Swansea University,
Swansea (U.K) SA1 8EN*

E-mail address: Sanjiv.sharma@swansea.ac.uk

Tel: 07915 381 689

Abstract

1 The fabrication of silicon in-plane microneedle arrays from a simple single wet etch step is
2 presented. The characteristic 54.7° sidewall etch angle obtained via KOH etching of (100) orientation
3 silicon wafers has been used to create a novel microneedle design. The KOH simultaneously etches
4 both the front and back sides of the wafer to produce V shaped grooves, that intersect to form a
5 sharp pyramidal six-sided microneedle tip. This method allows fabrication of solid microneedles with
6 different geometries to determine the optimal microneedle length and width for effective
7 penetration and minimally invasive drug delivery. A modified grooved microneedle design can also
8 be used to create a hollow microneedle, via bonding of two grooved microneedles together, creating
9 an enclosed hollow channel. The microneedle arrays developed, effectively penetrate the skin
10 without significant indentation, thereby enabling effective delivery of active ingredients via either a
11 poke and patch application using solid microneedles or direct injection using hollow microneedles.
12 This simple, scalable and cost effective method utilises KOH to etch the silicon wafer in-plane,
13 allowing microneedles with variable length of several mm to be fabricated, as opposed to out-of-
14 plane MNs, which are geometrically restricted to dimensions less than the thickness of the wafer.
15 These microneedle arrays have been used to demonstrate effective delivery of insulin and
16 hyaluronic acid into the skin.
17
18
19
20
21
22
23
24
25
26
27
28
29

Key words

30
31
32 Microneedle, drug delivery, silicon, fabrication
33
34
35
36
37
38
39
40
41
42
43
44
45
46
47
48
49
50
51
52
53
54
55
56
57
58
59
60
61
62
63
64
65

1.0 Introduction:

The skin, being the largest organ of the human body, offers several advantages as a route for drug delivery. These include a large surface area and avoidance of the first pass metabolism of the gastrointestinal tract, which consequently increases the bioavailability of the drug and minimises any side effects [1]. Currently, transdermal drug delivery (TDD) is achieved using either topical products or transdermal patches. However, TDD using these products is limited due to their physio-chemical properties that hinder their permeation through the lipophilic *stratum corneum* (SC), and their diffusion rate through the skin. To address these challenges microneedles (MNs) have been developed to penetrate the SC in a minimally invasive manner, creating “micro-conduits” that permit more facile transport of drugs into the skin tissue from the skin surface. The first silicon substrate based MNs were fabricated in 1998 using photolithography and deep reactive ion etching (DRIE) to form out-of-plane (OOP) 100µm cones. The application of these MNs increased the permeation of calcein through the skin >1000 fold [2].

Research groups have successfully established MN fabrication protocols that facilitate high throughput manufacturing, including the use of wet etching methods for silicon using etchants such as potassium hydroxide (KOH) or tetramethylammonium hydroxide (TMAH). Fabricating the MN in the in-plane orientation presents an efficient and flexible fabrication method, where the only restriction on the MN length and width is the diameter of the silicon wafer.

In-plane MN fabrication processes employing multi-step simultaneous KOH wet etch process have previously been reported [3], where, six solid MNs with geometrically different tips were fabricated by changing the angle measurement of the MN tip mask design. These included either 5°, 10° or 30° isosceles triangles or 10°, 70.5° or 90° degree right angled triangles mask designs. Using (110) orientated silicon wafers, the wet etch step produced vertically straight (111) side walls that although effective at creating a precise MN shaft, did not produce a sharp MN tip. Due to the straight (111) walls, the tip was formed was a blunt triangular prism, these thickness of which was equal to the thickness of the wafer. The authors found that the blunt tips hindered penetration and thus instead developed a modified jagged step design, to improve tip sharpness. However, this did not omit the creation of the triangular prism, and penetration efficiency was limited.

A novel and simple wet etch protocol for the fabrication of sharp in-plane MN from (100) silicon is presented, which involves a single wet etch step and can be employed for the fabrication of both solid and hollow MNs. Functionality of MNs with varying dimensions has been characterised through skin insertion and mechanical tests. Two drug compounds insulin and hyaluronic acid were chosen to demonstrate effective transdermal drug delivery into skin using the in-plane MN; MN facilitated

1
2
3
4
5
6
7
8
9
10
11
12
13
14
15
16
17
18
19
20
21
22
23
24
25
26
27
28
29
30
31
32
33
34
35
36
37
38
39
40
41
42
43
44
45
46
47
48
49
50
51
52
53
54
55
56
57
58
59
60
61
62
63
64
65

insulin delivery offers a pain-free, discreet, and convenient alternative to standard hypodermic needle injection in diabetic patients, whilst MN-assisted delivery of hyaluronic acid could facilitate improved delivery into the dermal space for cosmetic applications.

2.0 Methods and Materials

Unless stated otherwise, consumables used were purchased from Sigma Aldrich (Dorset, UK), these include methylene blue, FITC-insulin, FITC-Hyaluronic Acid, PBS tablets, HCL, papain, collagenase, papain buffer solution consisting of sodium acetate, EDTA (Ethylenediaminetetraacetic acid) and DTT (Dithiothreitol).

2.1 Microneedle fabrication

MNs were fabricated using boron doped, double side polished, 300 μ m thick (100) orientation silicon wafers with a thermal silicon dioxide layer grown on both the front and back (Silicon Materials, Germany). Negative photolithography resist Nlof2070 and developer AZMIF726 were purchased from Microchemicals GmbH. To spin coat the wafers, an EA Laurell WS-650 spin coater was used, while a SUSS MicroTec MA8 UV mask aligner (MA) that enables back side alignment, was employed to pattern the resist layers. An SPTS Technologies ICP system was used to etch a window in the silicon dioxide layer, exposing the silicon substrate, while silicon wet etching was completed with 44% potassium hydroxide (KOH) (Microchemicals GmbH). The in-plane silicon MN fabrication steps comprises of 5 steps, where on completion, the MNs are fully etch-released from the wafer to create instant use devices, with no requirement for wafer dicing. The five steps are detailed in figure 1.

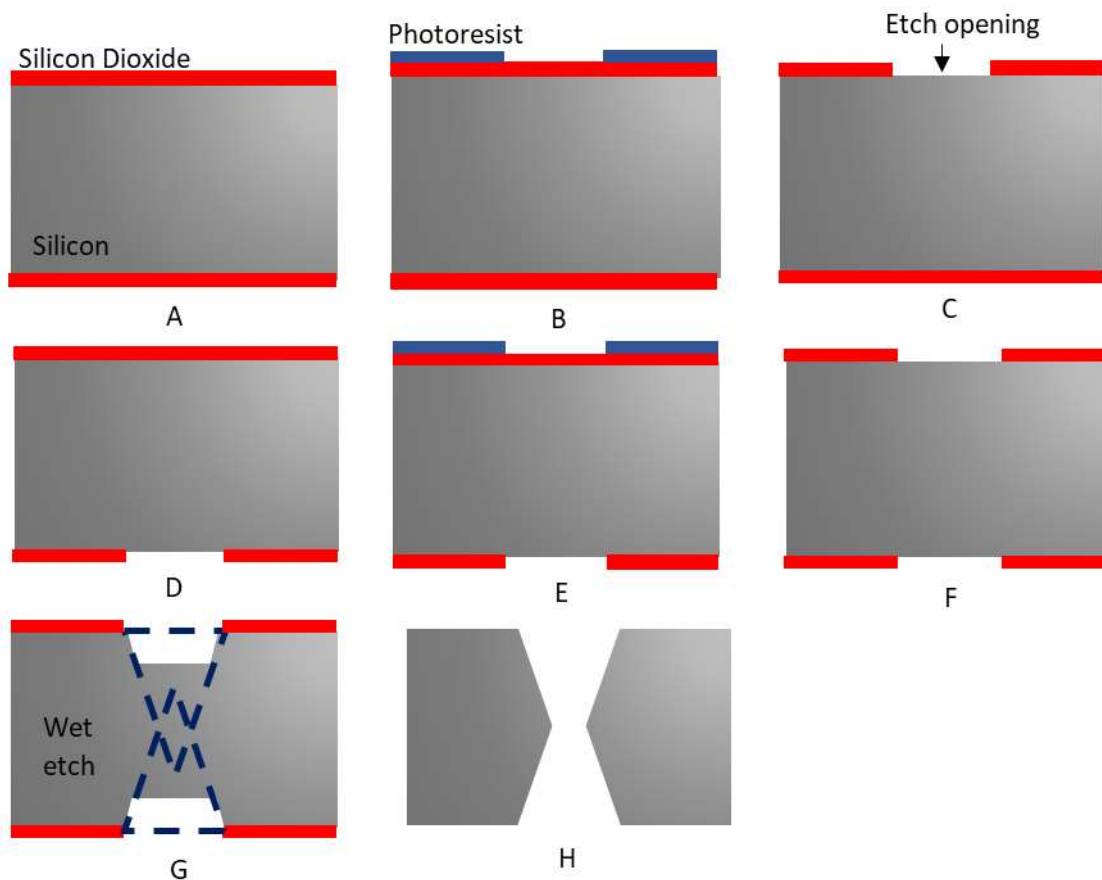


Figure 1. Schematic diagram showing cross-section of process steps for in-plane silicon microneedle fabrication. Silicon wafers are represented in grey, silicon dioxide is shown in red and the photoresist is shown in blue. A) 2.5 μm of silicon dioxide is deposited onto both sides of a 300 μm wafer using CVD. B) Photolithography processes are used to pattern devices onto silicon dioxide. C) The device pattern is etched into the silicon dioxide hard mask using ICP. D) The wafer is flipped. E) Photolithography is used to pattern devices onto the backside using alignment marks. F) The device pattern is etched into the silicon dioxide hard mark using ICP. G) The whole wafer is submerged into 44% KOH solution for etching, the dashed lines depict the etching process over 5 hours. H) The devices are removed from KOH solution.

2.2 Skin preparation and storage

Porcine skin obtained from Wetlab Ltd. Warwicks UK was prepared to full thickness for image analysis experiments by removing the muscle layer, or dermatomed to 500 μm thickness for Franz cell experiments on day of delivery. Excised human breast skin was obtained from surgical procedures under full ethical approval and informed patient consent (South East Wales Research

1
2
3
4
5
6
7
8
9
10
11
12
13
14
15
16
17
18
19
20
21
22
23
24
25
26
27
28
29
30
31
32
33
34
35
36
37
38
39
40
41
42
43
44
45
46
47
48
49
50
51
52
53
54
55
56
57
58
59
60
61
62
63
64
65

Ethics Committee Ref. 08/WSE03/55). Excised skin was transported, stored, and prepared as previously described [4].

2.3 Characterisation of solid and hollow microneedle array.

2.3.1 Image analysis

A scanning electron microscope (Hitachi S4800) was used to image the MNs, while an optical microscope (Keyence VHX-950F) combined with ImageJ software (Version 1.51k, National Institutes of Health, MD, USA) was used for skin image analysis.

2.3.2 Penetration characterisation

MN penetration into full thickness porcine skin, approx. 1mm, was assessed via methylene blue staining (for 1- minute duration). Human skin was used for characterisation of the micro-conduits created in the skin after MN insertion via optical coherence tomography (OCT).

2.3.3 Microneedle injection analysis

Hollow MNs were used to inject FITC-insulin into porcine skin. Post injection skin was immediately frozen in liquid nitrogen and cross sectioned to a thickness of 10 μ m using a cryostat (Leica, Milton Keynes, UK). To visualise the skin sections a fluorescent microscope (Zeiss Axio Imager M1, Germany) was used.

2.3.4 Microneedle mechanical testing

To analyse the mechanical strength of the MNs, the compression force to fracture in relation to displacement was measured with an axial compression analyser (Hounsfield/Tinius Olsen H1KS, PA, USA) with a 50N load cell descending at a rate of 4.5mm/sec. As moderate thumb pressure is classified as 10N [5], this acted as a baseline to determine whether the MNs had sufficient mechanical strength. Each test was run in triplicate.

2.3.5 Drug Delivery of Insulin and Hyaluronic acid

In vitro drug permeation assays were conducted using Franz cell apparatus (n=3) (Cole Palmer, UK). The donor chamber was omitted, and the receptor chamber was filled with 0.01M PBS, equipped with a magnetic stirrer and set at a controlled temperature of 32°C to mimic the skin temperature. FITC-Hyaluronic acid (MW ~800,000Da) was diluted to 1mg/ml in cold dH₂O and left overnight in a

1 dark fridge at 2-8°C to fully dissolve, in line with the manufacturer's instructions. FITC-insulin (5,808
2 Da) was dissolved in 0.01M HCl to a final concentration of 0.1mg/ml. Porcine skin was shaved and
3 dermatomed to a thickness of 500µm and its integrity confirmed through electrical resistance
4 measurements. Each skin sample was treated with a solid MN array, of either 300µm or 600µm MN
5 length, five consecutive times before being clamped between the donor and receptor compartments
6 of the Franz cell. 200µl of either FITC-insulin or FITC-Hyaluronic acid was applied to the skin surface,
7 and the cumulative concentration in the receptor chamber was analysed over 11 time points (5, 10,
8 15, 30 minutes and 1, 2, 4, 6, 8, 10, 12 and 24 hours). Each sample withdrawn from the receptor fluid
9 was analysed in triplicate via a fluorescent spectrophotometer (FLUOstar Omega, BMG labtech) at a
10 detection wavelength of 495nm, to determine the concentration of FITC-insulin and FITC-HA in
11 comparison to a standard calibration curve.
12
13
14
15
16
17
18
19
20
21

22 **2.4 Drug retention within skin**

23
24 To further investigate the permeation profile of drugs into and through the skin, any remaining drug
25 was extracted from the skin samples through tape strip and homogenisation analysis. Tape strip
26 analysis was conducted by subjecting the skin to 10 rounds of tape stripping [6]. The first tape strip
27 was placed into 4ml of 0.01M PBS, while tape strips 2-10 are pooled together and submerged in 4ml
28 of 0.01M PBS. All samples were covered in foil to prevent photobleaching and rotated on a roller-
29 mixer overnight. To extract the drug concentration from the remaining skin sample, papain or
30 collagenase enzymes were prepared for skin homogenisation, i.e., to break down the skin structure
31 and release the drug into solution. 2mg/ml of papain was diluted in a buffer consisting of 20mM
32 Sodium Acetate, 1mM EDTA (Ethylenediaminetetraacetic acid) and 2mM DTT (Dithiothreitol) at pH
33 6.8 and homogenised the skin at 60°C. Collagenase was dissolved in 0.01M PBS and homogenised
34 the skin at 37°C. Skin samples treated with FITC-insulin were placed in 4ml of collagenase solution
35 while Hyaluronic acid samples were homogenised in papain. Samples were stored overnight at the
36 enzyme's corresponding temperature in the dark to prevent photobleaching. To remove debris, the
37 samples were spun in a centrifuge, at 3000RPM for 10 minutes, and the supernatant removed for
38 analysis through fluorescence spectrophotometry using an excitation wavelength of 495nm.
39
40
41
42
43
44
45
46
47
48
49
50

51 To analyse the concentration of each drug from the respective tape strips, homogenate or Franz cell
52 chamber, the results are displayed as a stacked bar graph. Here each different shade of grey
53 correlates to the skin layer from which the drug is recovered, with the darkest grey representing the
54 percentage of drug recovered from the first tape strip and hence dye remaining on the skin surface;
55 the second darkest grey represents the percentage recovered from 2-10 consecutive pooled tape
56 strips, to determine the amount of drug that has partitioned into the SC; the next section reflects the
57
58
59
60
61
62
63
64
65

1 percentage of drug quantified from the homogenate and thus the amount of drug that has
2 successfully permeated into the viable epidermis and finally, the lightest grey represents how much
3 drug has been recovered from the Franz cell receptor compartment, and thus would be available to
4 the lower epidermis and potentially the systemic circulation.
5
6
7
8

9 **2.5 Statistical analysis**

10 The means of multiple data sets from the cumulative drug graphs were analysed and compared
11 using student's *t*-test or one-way ANOVA with Microsoft Excel and SPSS software, followed by
12 Tukey's *post hoc* test. A P-value of <0.05 was considered significant.
13
14
15
16
17
18
19
20

21 **3.0 Results and discussion**

22 **3.1 Microneedle fabrication**

23 A scanning electron micrograph (SEM) of the MN cross-section (Figure 2A and C), confirms that
24 simultaneously etching the front and reverse of a silicon (100) wafer with KOH produces an etch
25 profile formed from the characteristic anisotropic convex (110) sidewalls that intersect into a
26 pyramid to form a MN tip (highlighted in blue). In addition, figures 2B and D demonstrate that the
27 (111) sidewalls along the MN shaft have also intersected, to form a hexagonal prism shaped shaft
28 from four (111) (highlighted in red) and two (100) planes (blue). The thickness of the MN is 300µm,
29 corresponding to the original wafer thickness. A variety of MN devices with different dimensions
30 were created to analyse the effect of KOH etching on the MN structure. MNs with heights measuring
31 1200, 1100, 1000, 900, 800, 700, 600, 500, 400 and 300µm and with a consistent width of 300µm
32 were created. Furthermore, to analyse how the etch affected the width of the MN, MNs of 700µm in
33 height and with widths of either 700, 600, 500, 400, 300, 200, 100, 50 and 25µm were created.
34 Different heights and widths were evaluated to determine the optimal dimensions for sufficient skin
35 penetration and drug delivery, i.e., if the MN is too short it would not effectively penetrate the SC,
36 while too long could penetrate too deeply and cause pain. Alternatively, if the MNs were too wide,
37 the angle at which the tip intersects is too large, creating a less-sharp tip that may not penetrate the
38 SC. Initial post etch observations using SEM, indicated that the height of all MNs were less than their
39 respective original photolithography mask designs, while the width dimension increased from the
40 original mask design, in relation to successfully creating the MN tip.
41
42
43
44
45
46
47
48
49
50
51
52
53
54
55
56
57
58
59
60
61
62
63
64
65

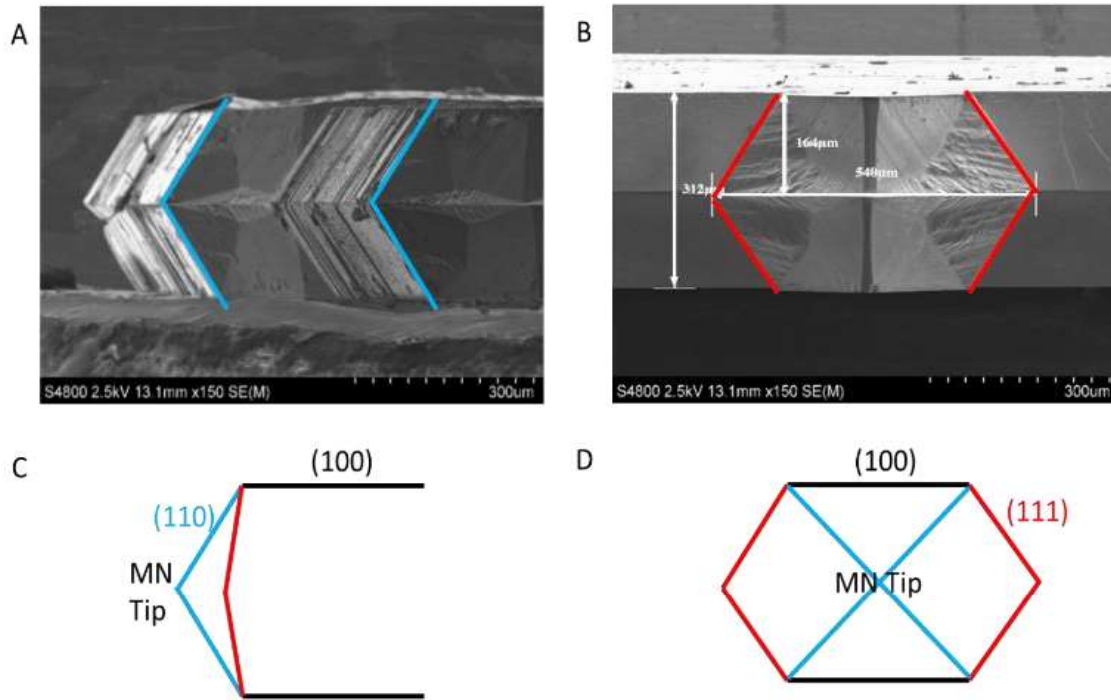


Figure 2. SEM of solid in-plane MN from the (100) cross section to demonstrate (A) the subsequent tip created from (110) planes (blue) (B) orientated to look down the shaft of the MN, showing the hexagonal shaft shape created from the 54.7° angle (111) planes (red) to measure, 540µm wide and 312µm deep. C and D are schematic representations of SEM images A and B, to clarify etched plans and MN orientations.

Figure 3A shows the formation of the MN tip. Due to the etch exposing the (110) planes to form the pyramid shaped tip, the length of the MN consequently reduces by approximately 313µm from its original rectangular mask designed length. For example, if the mask MN design measured 1000µm in length, the resulting MN would measure 682µm, therefore this needs to be considered when designing MN photolithography masks. Figure 3B shows that the width of the original MN mask patterned onto the wafer is maintained in the (100) plane orientation (outlined in yellow). However, as the shaft of the MN is created from the etch exposing the (111) planes intersecting at 54.7°, these planes increase the width of the MN by 179µm (red arrows). Additionally, as a result of the increased width, the angle at which the tip is formed in the (100) orientation also increases (figure 4). If the angle becomes too large, it is likely to inhibit penetration.

15
16
17
18
19
20
21
22
23
24
25
26
27
28
29
30
31
32
33
34
35
36
37
38
39
40
41
42
43
44
45
46
47
48
49
50
51
52
53
54
55
56
57
58
59
60
61
62
63
64
65

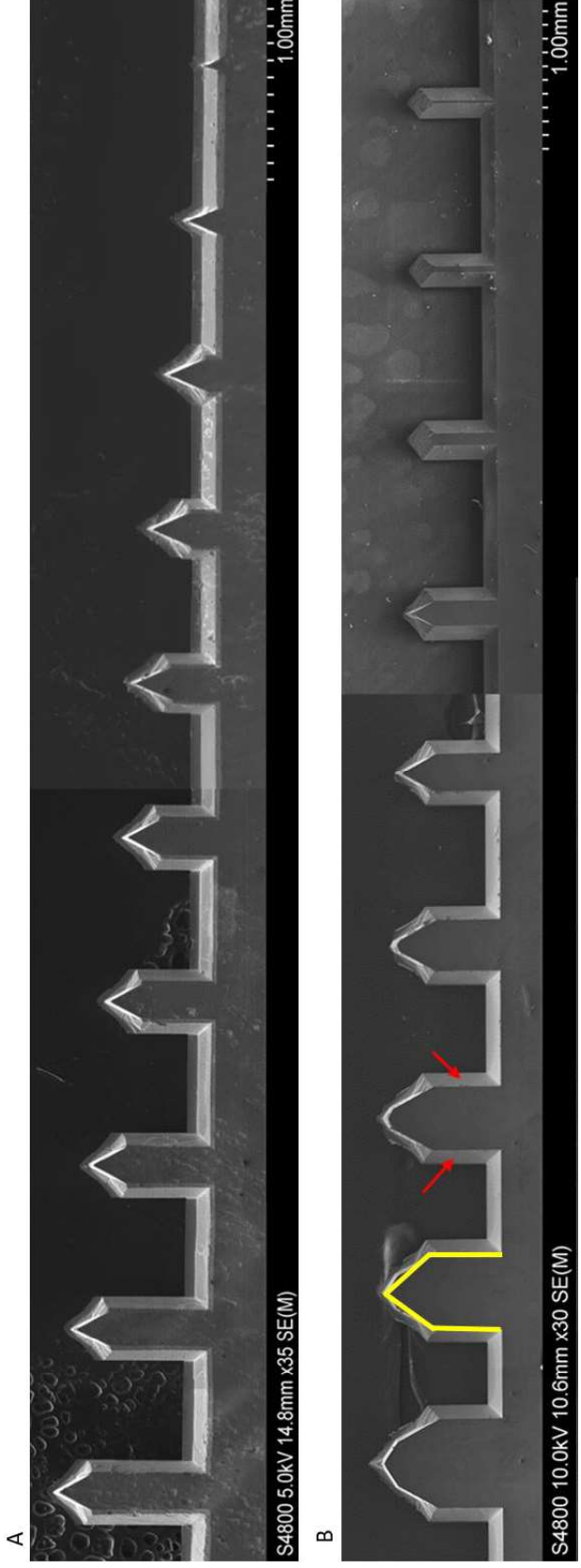


Figure 3 SEM images of solid in-plane MNs fabricated to (A) different heights and (B) different widths. Yellow outline highlights the original mask design, while the arrows show how the (111) planes intersect to increase the width.

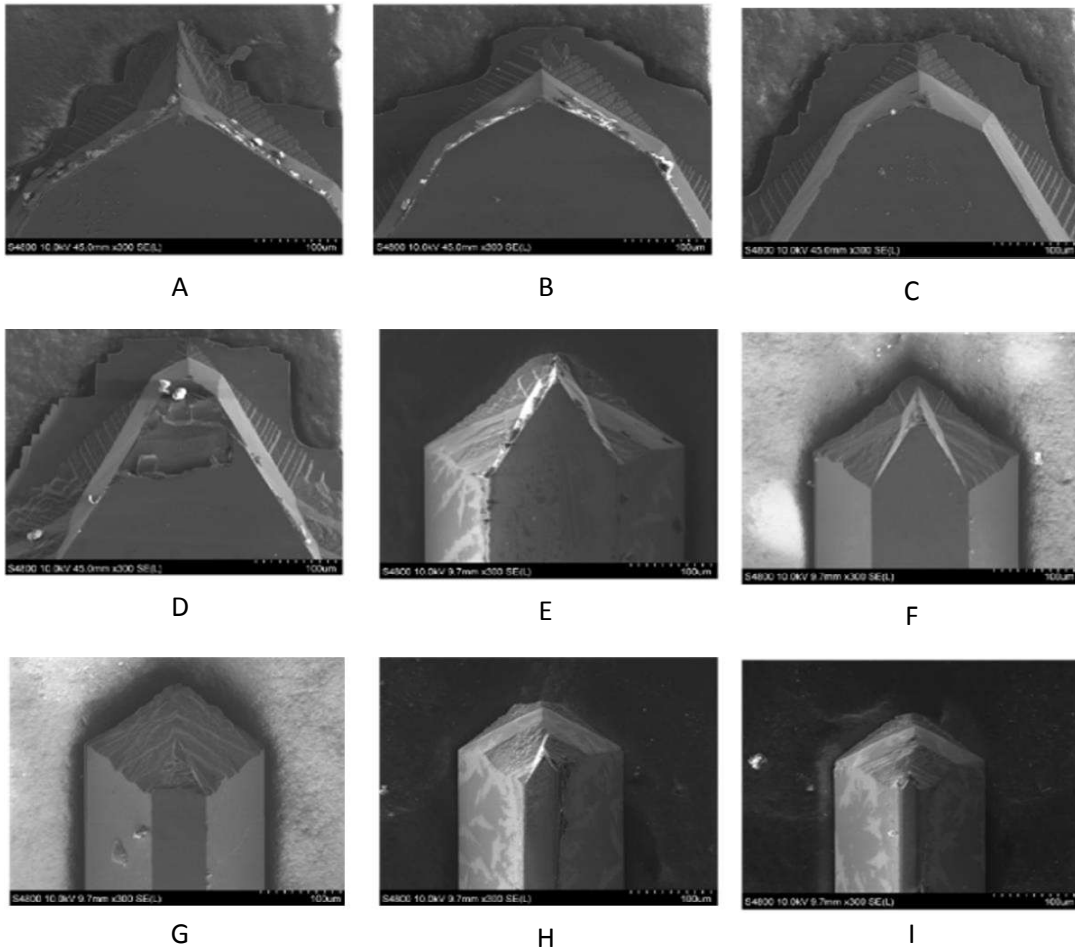
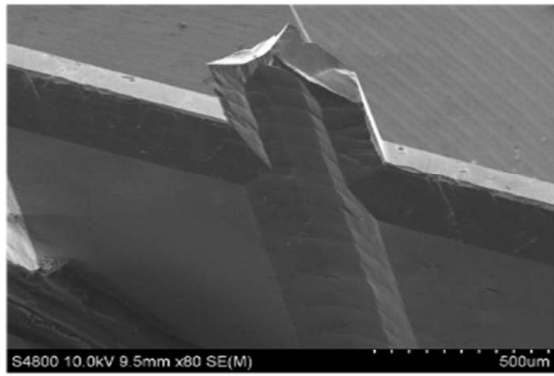


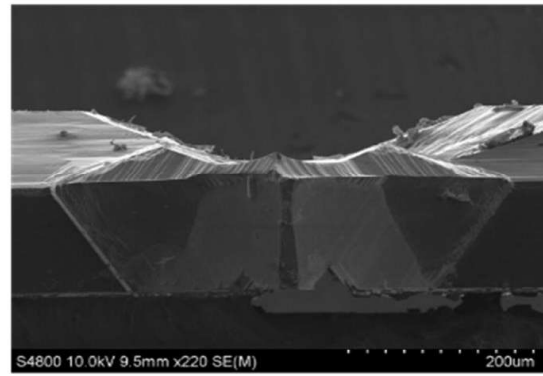
Figure 4. SEM images of solid in-plane MNs to examine the MN tip angles with varying MN width (A) 700 μ m 117° (B) 600 μ m 123° (C) 500 μ m 122° (D) 400 μ m 73° (E) 300 μ m 60° (F)200 μ m 57° (G) 100 μ m 51° (H) 50 μ m 53° (I) 25 μ m 57°

3.2 Hollow microneedles

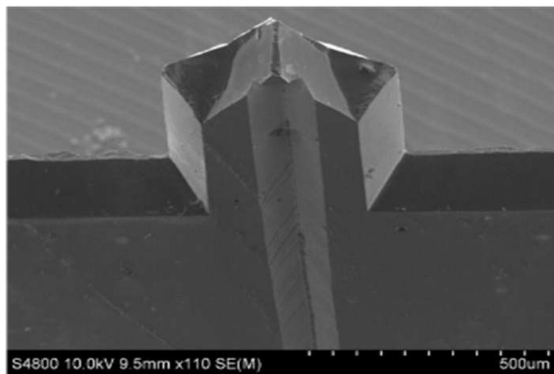
To fabricate a hollow version of the in-plane MN, a modified photolithography mask was used to incorporate a hollow channel from the tip of the MN, that runs centrally along the length of the MN device. This channel is formed from the (111) planes inversely etching at 54.7° to form a V shaped groove. Two different channel widths were designed on the mask to produce either 100 μ m or 200 μ m channels (Figure 5). The 200 μ m channel mask width produced a channel that measures approximately 231 μ m wide and 67 μ m deep (Figures 5A & B). The base of the channel is flat as the 54.7° (111) sidewalls have not etched deep enough to intersect and create the characteristic V shaped channel. In contrast, the 100 μ m channel mask width formed a groove measuring 134 μ m wide and 88 μ m deep (Figure 5C & 5D), with the (111) side walls intersecting to form a V-shaped channel. Therefore, the width of the channel mask dictates the depth that the channel that can be etched, which would influence the volume, pressure, and rate of injection.



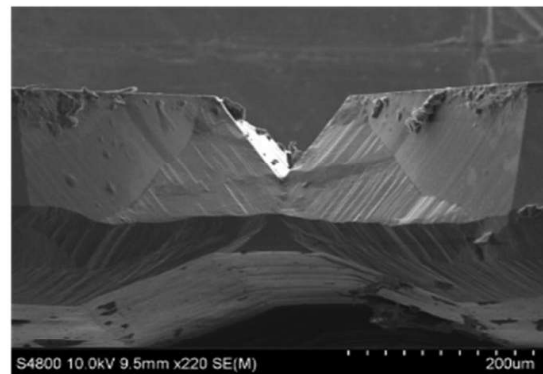
A



B



C



D

Figure 5. Scanning electron microscope images of a grooved microneedle channel with a starting mask width of (A-B) 200µm (C-D) 100µm. (B) and (D) are orientated to view down the channel and examine the KOH etched shape.

3.2 Characterisation of microneedle penetration and mechanical tests

To assess how varying the heights and widths of MN affect skin penetration, characterisation was performed using methylene blue staining and OCT analysis, after insertion with different height and width MN arrays, as listed in table 1. Each array consisted of five MNs.

Table 1 Different microneedle height and widths measured after KOH etching

<u>Microneedle ID</u>	<u>Height (μm)</u>	<u>Width (μm)</u>
H1	66	450
H2	245	450
H3	392	450
H4	550	450
H5	784	450
H6	1150	450
W1	550	225
W2	550	252
W3	550	295
W4	550	378
W5	550	450
W6	550	586
W7	550	665

3.2.1 Insertion tests

Methylene blue dye was applied to porcine skin following MN application to detect whether the MNs were sharp enough to breach the *stratum corneum* (SC). The staining results show porcine skin treated with MNs of varied height (Fig. 6A). Longer MNs penetrate through the SC more effectively. However, the full length of the MN cannot completely be inserted into the skin. The penetration efficiency (PE) is calculated from the number of methylene blue stained dots in relation to the number of MNs, in this case a 1 x 5 MN array applied 4 times produces a maximum number of 20 stained areas. The shortest MNs, model H1, were not long enough to penetrate through the SC so no staining was observed. Increasing the MN length (models H2 and H3), yielded some staining, but with an inconsistent, unreliable PE. Models H4 and H5 produced penetration profiles with clear individual MN penetration that upon repetition gave 100% PE. Increasing the MN length further (model H6) created less distinguishable PE due to the MB stain bleed within the tissues, which may be due to increased SC damage.

The width of the MN after KOH etching increases by approximately 179 μm irrespective of the original mask width design. MNs with varying widths were tested using methylene blue staining, (fig. 6B). The thinnest MN models W1 & W2 show 60% PE, while models W3-W5 all successfully produced clear 100% PE profiles. MN model W6 with a width of 586 μm , produced a slightly lower PE

1 of 85%. The largest MN, model W7 showed very little MB staining, suggesting the MNs were too
2 wide to penetrate. However, areas that were stained produced smaller sized marks, comparable to
3 the penetration marks created by the smaller width MNs. Although wider MNs with larger MN tips
4 maintain the 57.4° angle in the (111) orientation, the thicker tips are less sharp in the (100) axis, thus
5 preventing them from penetrating through the SC. Furthermore, although the smallest MN models
6 W1 and W2 somewhat penetrated the skin, their fragility made them prone to breaking before and
7 during insertion meaning 100% PE was not achieved. The staining tests demonstrated that the
8 optimal MN widths were 200 and 300µm, demonstrating no breakages and successful penetration
9 through the SC.
10
11
12
13
14
15

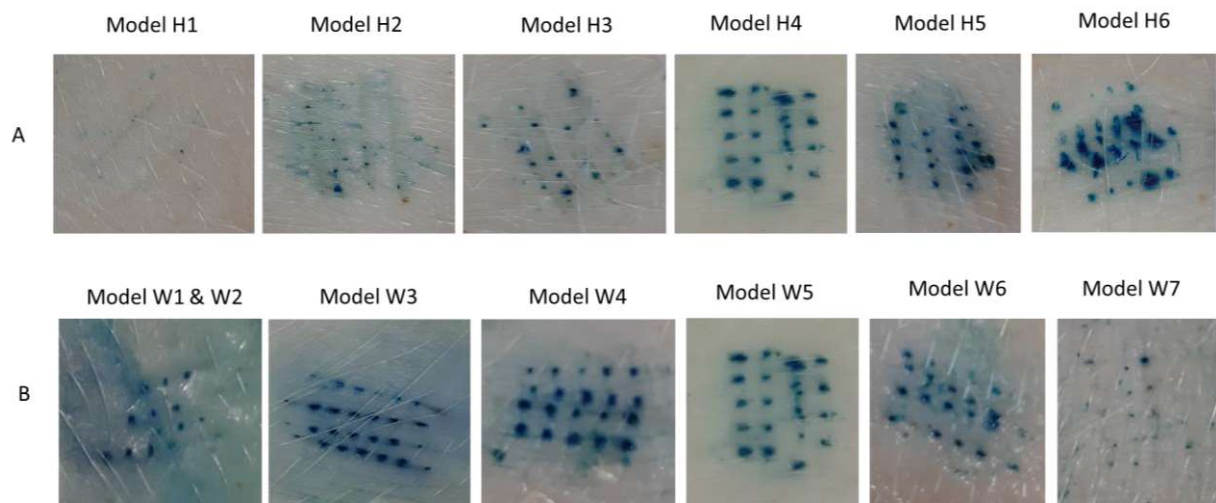


Figure 6 Methylene blue staining of porcine skin treated with MNs of (A) different heights and (B) different widths, four consecutive times. Each MN array consists of five MNs. Successfully penetration through the *stratum corneum* is indicated by a blue dot.

3.2.2 Optical coherence tomography

Optical coherence tomography (OCT) was used to assess the morphology of the microchannels created by the MN after penetration. Results show that the longer MNs penetrated deeper into the skin (Figure 7A-D), whereas the shortest MN measuring 66µm, did not penetrate at all (Figure 7E). Penetration depths for subsequent MN models H2-H6, taken in triplicate, measured 218, 294, 394, 453 and 462µm, respectively as shown in figure 7. However, when calculating the percentage insertion i.e., how much of the MN length was inserted into the skin, the results found that 40% of model H6 penetrated, 58% of model H5 and 72%, 75% and 89% for models H4, H3, and H2, respectively. Even though the longest MN penetrated the deepest into skin, it had the lowest MN length / penetration depth ratio. This may be due to the elasticity of the skin, consequently closing the channels upon MN removal, thus underestimating the actual depth of penetration. Figure 7 also

1 demonstrates that smaller MN widths, models W1-W3, enable the deepest penetration into the
2 skin, whilst the largest widths with MN models W6 and W7, did not penetrate through the SC, only
3 indenting the skin. The widest MN to successfully puncture the skin was model W5, which created a
4 microchannel depth of 364 μ m; an insertion percentage of 66% of the MN height. However, the
5 width of the microchannel insertion measured 824 μ m, 183% wider than the MN itself, which is likely
6 to be from a combination of penetration plus indentation. The microchannel depths of models W1-
7 W4 measured approximately 428 μ m, 403 μ m, 411 μ m, and 277 μ m with insertion percentages of 78%,
8 73%,75%, and 50% respectively. The results indicate that smaller width MNs can penetrate deeper
9 into the skin, reaching the upper dermal regions, whilst larger MN widths produce unreliable and
10 inconclusive disruption of the SC, with indentations or shallow epidermal insertion observed.
11
12
13
14
15
16
17
18

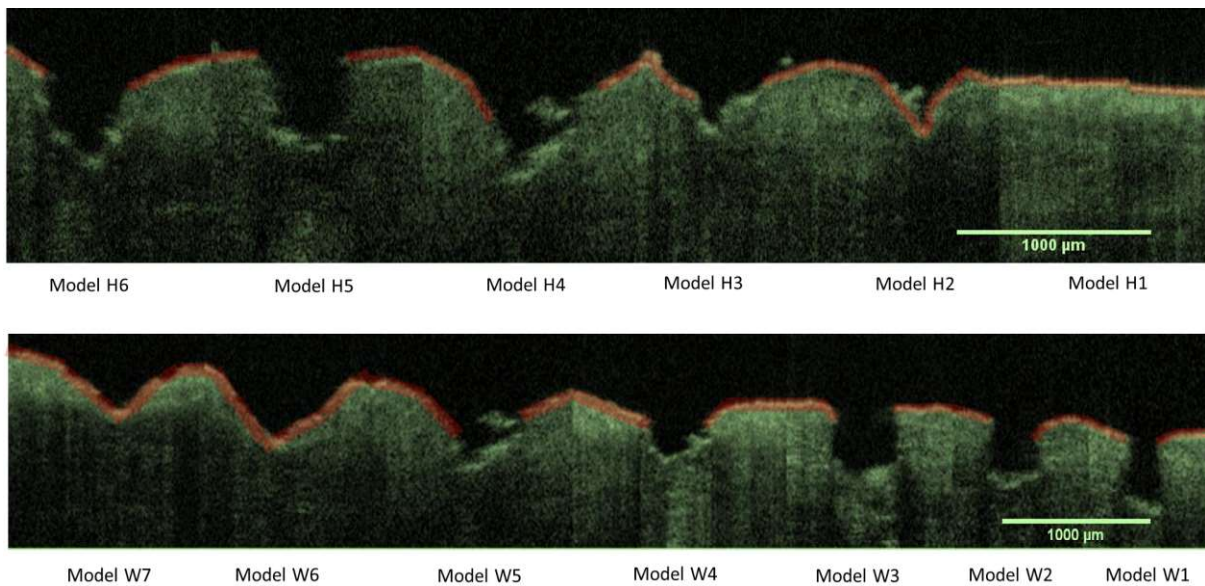


Figure 7 OCT images of human skin after treatment with MNs of different heights (model H1 –H 6) and different widths (models W1- W7) to create subsequent micro-channels.

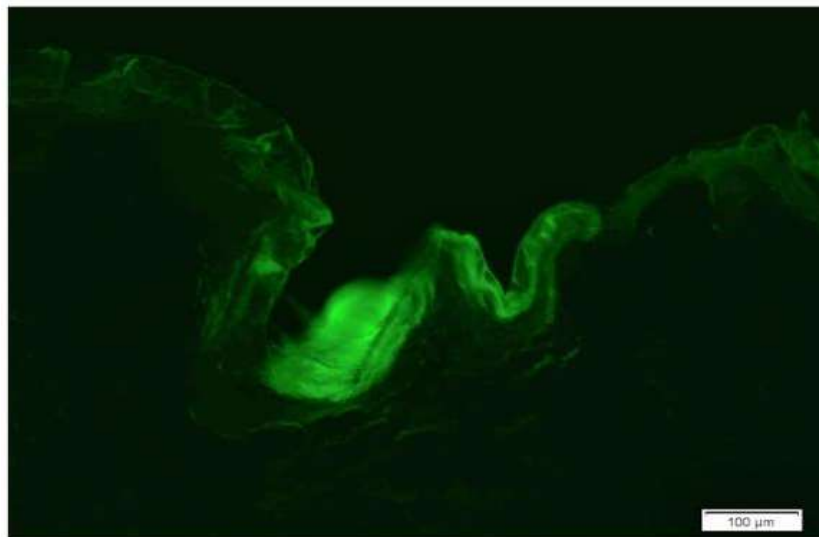
3.2.3 Mechanical testing

To overcome the skin barrier and deliver drugs efficiently, it is crucial that the MNs do not fracture with insertion force, which has been reported in previous literature as approximately 10N [5]. Compression forces of greater than 10N, applied to MNs of different heights were sustained by all MN lengths, with the exception of the longest MN, model H6, which fractured at a compression distance of <100 μ m, in line with the tip crumbling or chipping. As the compression platform is composed of hard metal with little elasticity or movement, it is possible that all MNs will be able to withstand a greater force upon application to the softer, elastic skin samples. MN models W3- W6 were compressed in triplicate to evaluate the effects of MN width on mechanical strength. All MNs tested were able to withstand forces of 10N or above and therefore should not fracture upon skin

1 penetration. Additionally, the mechanical strength of the MNs increased with increasing width, as
2 fewer fractures were observed for these wider MNs. This could be explained due to larger
3 distribution of force per unit volume of the larger MN tip, enabling these MNs to tolerate a larger
4 load force.
5
6
7
8
9

10 **3.2.4 Hollow microneedles**

11 Hollow MNs created from the 200 μ m mask design, were fabricated to explore their injection
12 potential. FITC-insulin loaded syringes were connected to a syringe pump to maintain an injection
13 flow rate of 10 μ l/min into porcine skin. Figure 8 suggests successful injection into the deeper skin
14 layers as, despite the observed skin autofluorescence, a stronger green fluorescence, due to FITC-
15 insulin, appears to be predominantly located near the base of a MN-created microchannel.
16
17
18
19
20
21
22

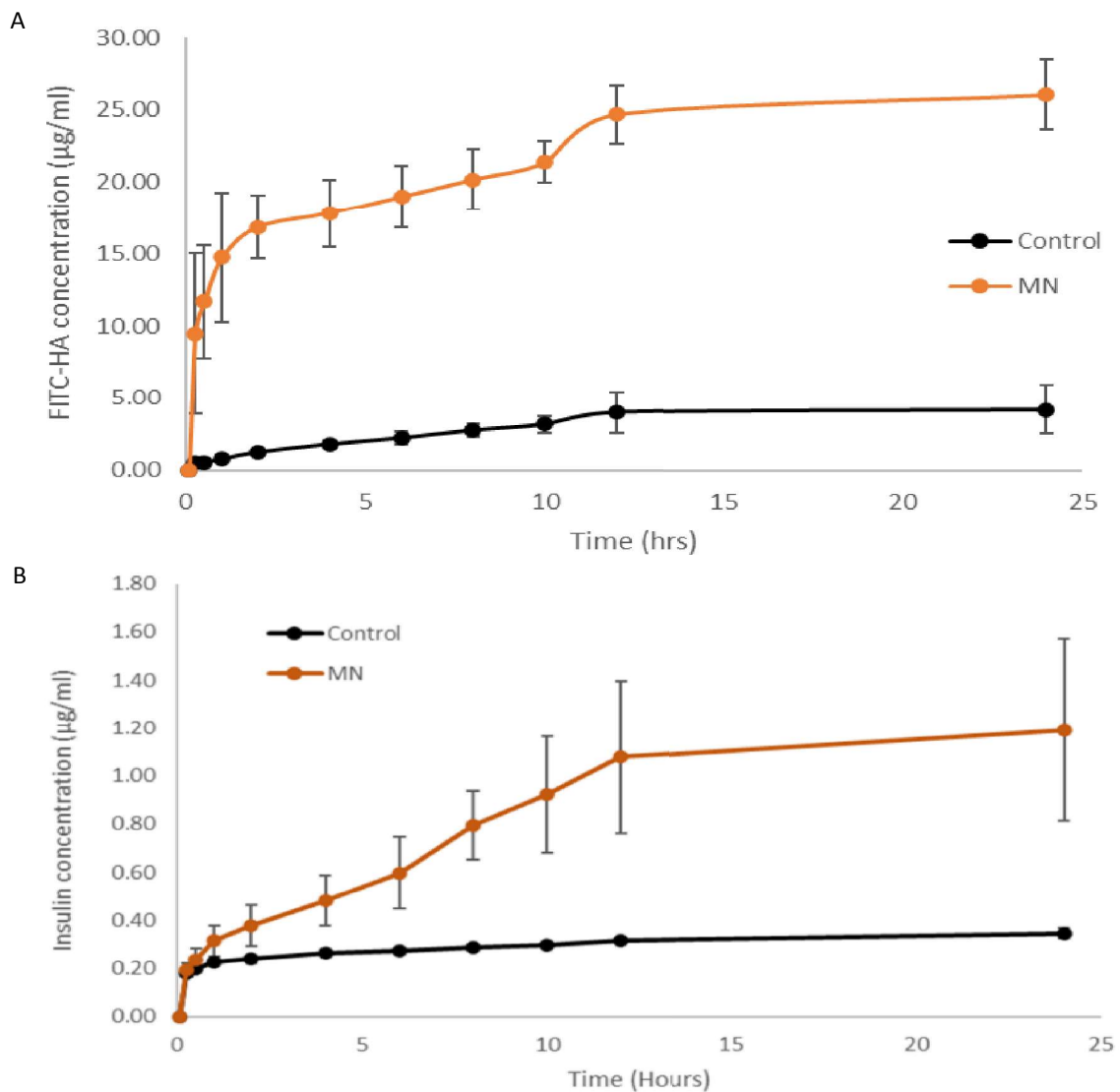


41
42 Figure 8 Fluorescent microscopy image of FITC-insulin injected into porcine skin via in-plane
43 200 μ m grooved MNs
44
45

46 **3.2.4 *In vitro* drug delivery**

47 Optimised MN dimensions (278 μ m wide and either 300 or 600 μ m in height), were selected for their
48 ability to penetrate either to the shallow epidermis or deeper upper dermis, for drug delivery
49 applications. *In vitro* Franz cell testing, after MN surface application, was conducted using the
50 shorter MNs for hyaluronic acid delivery in relation to cosmetic applications, whereas longer MNs
51 were used to in deliver insulin, where targeting delivery into the deeper skin tissues could promote
52 systemic uptake. Both HA and insulin are hydrophilic and larger than 500Da, meaning that the
53 molecules are unable to pass the lipophilic SC barrier unaided, making them ideal candidates for
54
55
56
57
58
59
60
61
62
63
64
65

1 MN-assisted delivery. Time-point samples taken from the Franz cell receptor chamber are used to
2 produce the cumulative drug concentration graphs in figure 9. Figure 9A demonstrates that the
3 majority of HA diffused into the Franz cell receptor within the first hour, with a flux rate of
4 59.59 $\mu\text{g}/\text{cm}^2/\text{h}$, suggesting the release was rapid with MN treatment in comparison to the control
5 (HA applied without any MN treatment). Figure 9B shows that the flux rate of insulin, 1.13 $\mu\text{g}/\text{cm}^2/\text{h}$,
6 is significantly slower than HA delivery, however, it is still greater than the insulin control. Final
7 cumulative concentrations from the Franz cell receptors of 25.03 $\mu\text{g}/\text{ml}$ for FITC-HA at and 1.19 $\mu\text{g}/\text{ml}$
8 for FITC-insulin, were both statistically different to their controls of drug application on the skin
9 without MN application ($P < 0.000006$ and $P = 0.00318$ respectively), confirming that MN-assisted
10 delivery facilitated drug permeation of skin.



57 Figure 9 Franz cell receptor cumulative concentration graphs of (A) FITC-HA and (B) FITC-insulin
58 permeation across porcine skin with MN assistance, against non-MN treated skin controls
59
60
61
62
63
64
65

1
2
3
4
5
6
7
8
9
10
11
12
13
14
15
16
17
18
19
20
21
22
23
24
25
26
27
28
29
30
31
32
33
34
35
36
37
38
39
40
41
42
43
44
45
46
47
48
49
50
51
52
53
54
55
56
57
58
59
60
61
62
63
64
65

Despite a percentage of the original drug concentration applied to the Franz cell diffusing into the receptor compartment, some drug remains trapped in the skin layers following topical application. This can be quantified in the SC and underlying skin layers by tape stripping the upper layers and analysis of the homogenised lower skin layers. Figures 10 and 11 show the results of tape stripping experiments, performed using OCED guidelines [6]. Figure 10A demonstrates the percentage of FITC-HA calculated from each skin layer for the control and MN treated skin. The control profile reveals that on average 62% (153.16µg/ml) of the FITC-HA is retained unabsorbed on top of the skin and 31% (77.31µg/ml) had partitioned into the SC, yielding a combined total of 93% of FITC-HA trapped on the skin surface and in the SC. This confirms that FITC-HA penetration through porcine skin without MN treatment, is negligible. In comparison, the MN treated skin had 8% (17.93µg/ml) of the FITC-HA remaining unabsorbed on the skin, while 34% (81.31µg/ml) partitioned into the SC, equating to a total of 42% which has not been able to penetrate beyond the SC. However, the largest FITC-HA percentage recovered was 48% (113.57µg/ml) which was found within the homogenised skin. Combining this with the concentration found in the receptor fluid (11%), equates to an overall successful permeation concentration of 139.60µg/ml (59%). These results demonstrate that FITC-HA permeated through the SC to reside primarily in the epidermal region of the skin.

The FITC-insulin graph in figure 9B, shows that only 2% of the original dosage was recovered from the Franz cell receptor in the control sample. Figure 10B shows the full diffusion profile incorporating the tape strips and homogenisation results for FITC-insulin administration with MNs and the subsequent control, which accounts for the remaining dosage. Analysing the FITC-insulin that did permeate the skin after MN treatment, showed that only 9% diffused into the receptor fluid, while other skin layers had a final concentration of 27% (non-absorbed), 27% (tape strips) and 37% (homogenate). Although small doses of FITC-insulin were detected in the receptor fluid, the homogenate layer contained the largest concentration of 4.6µg/ml which, once combined, demonstrates a total successful drug permeation of 46%. The control sample results showed that 63% of the FITC-insulin stayed on the surface of the skin with only 21% partitioning into the SC, confirming that FITC-insulin did not efficiently penetrate through the skin unaided to any significant degree.

This study examined whether FITC-insulin could permeate into the epidermal region and thus be recovered in the skin homogenate and the Franz cell receptor chamber to target systemic delivery. Although some successful permeation was observed, a larger percentage of FITC-insulin remained on top of the SC or partitioned into it, rendering it unavailable to the systemic circulation. Insulin not only has a large MW, but also low solubility at physiological pH of 7.4 [7], adding another challenge to delivery. It is generally accepted that a non-ionised species of an acidic or basic molecule is more

permeable across the skin barrier than the ionised form [8]. Thus, penetration across the SC is affected by the physiochemical properties of the drug and the degree of ionisation. However, the SC has an acidic pH for protection against external pathogens. The pH ranges from 4.5 to 5.0 in the outer SC layers, termed the “acid mantle” and approaches a neutral pH in the lower layers and the epidermis [8]–[11]. As insulin is soluble at an acidic pH [12], the acidic nature of the SC may be preferentially retaining insulin in the SC layer because of its higher solubility in the more acidic environment of the SC, compared to deeper skin layers where the pH approaches neutrality. This solubility issue is suggested to prevent permeation [13], providing an initial purported explanation for the higher percentage (54%), of FITC-insulin recovered from the skin surface and the SC, through tape strip analysis.

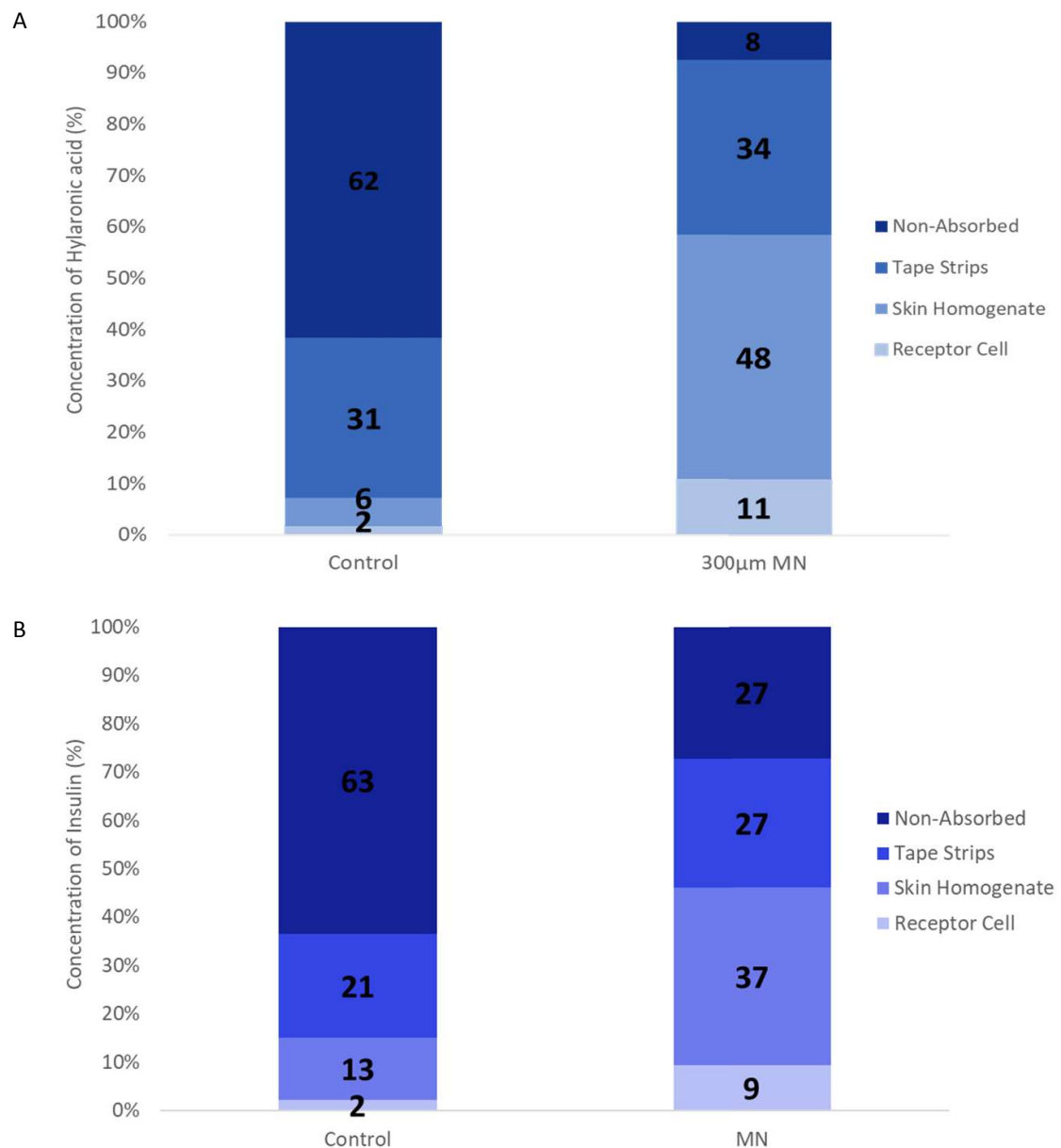


Figure 10 stacked bar graph showing permeation profile of (A) FITC-Hyaluronic acid and (B) FITC-insulin through porcine skin with and without MN treatment.

Conclusion

Novel in-plane MNs were fabricated from simultaneous front and back side etching of a (100) silicon wafer in KOH solution, utilising the characteristic (110) and (111) 54.7° angled planes to create the MN tip. This fabrication method has also been used to demonstrate different aspect ratio MNs which enable targeted drug delivery depths. By utilising KOH etching, the fabrication process is low-cost and scalable. In addition, it was demonstrated that by changing the mask design, hollow MNs can be fabricated using the same KOH etching method.

Through mechanical testing it was established that the primary mechanism of failure for the MNs was compression at the tip of the MN causing it to crumble, chip or blunt. Without the support of a wider MN, application of higher forces saw longer MNs ultimately fracture at the shaft and at their base. However, all MN geometries were mechanically strong enough to withstand at least 10N of force; equivalent to thumb pressure insertion into skin.

Characterisation of different MN geometries confirmed that MNs measuring >66µm in height and <460µm in width are suitable for effective skin penetration. The histological sections confirmed that a hollow channel etched along the MN shaft can facilitate the delivery of FITC-insulin into the skin. The varied length MNs may allow for targeted, application-dependent drug delivery to specific skin depths. MNs of different heights were used for testing the delivery of two large molecular weight molecules, HA and insulin, into porcine skin *in vitro* following MN application. MN heights measuring 300µm successfully delivered FITC-HA to the shallower epidermis to facilitate targeted local delivery, suitable for cosmetic applications. Longer, 600µm MNs, were used to deliver insulin. FITC-Insulin delivery did not yield such a high degree of skin permeation into the Franz cell or the deeper epidermis as FITC-HA. This is suggested to be related to the larger MW and acidic solubility of insulin, restricting insulin diffusion into the deeper skin layers. Future studies will employ hollow MNs for direct injection of FITC-insulin into deeper skin layers.

Conflicts of interest

There are no conflicts of interest to declare.

Research ethics

Full ethical approval and informed patient consent was confirmed under local research ethics committee reference 08/WSE03/55., for the use of human breast tissue in OCT experiments.

Author Contributions

Olivia Howells: Conceptualization, Methodology, Formal Analysis, Investigation, Original writing,

1
2
3
4
5
6
7
8
9
10
11
12
13
14
15
16
17
18
19
20
21
22
23
24
25
26
27
28
29
30
31
32
33
34
35
36
37
38
39
40
41
42
43
44
45
46
47
48
49
50
51
52
53
54
55
56
57
58
59
60
61
62
63
64
65

Review and Editing. Gareth Blayney: Etching Methodology. Benedetta Gualeni: Investigation, Review and Editing. James Birchall: Review and Editing. Pey F. Eng: Funding acquisition. Human Ashraf: Funding acquisition. Sanjiv Sharma: Review and Editing, Supervision. Owen J, Guy: Funding acquisition, Conceptualization, Review and Editing, Supervision.

Acknowledgements

We would like to acknowledge funding from Knowledge Economy Skills Scholarships (KESS), a pan-Wales higher level skills initiative led by Bangor University on behalf of the HE section in Wales.



References

- [1] S. Fakhraei Lahiji, Y. Kim, G. Kang, S. Kim, S. Lee, and H. Jung, "Tissue Interlocking Dissolving Microneedles for Accurate and Efficient Transdermal Delivery of Biomolecules," *Sci. Rep.*, vol. 9, no. 1, pp. 1–9, Dec. 2019.
- [2] S. Henry, D. V. McAllister, M. G. Allen, and M. R. Prausnitz, "Microfabricated microneedles: A novel approach to transdermal drug delivery," *J. Pharm. Sci.*, vol. 87, no. 8, pp. 922–925, 1998.
- [3] M. Jung, D. Jeong, S. S. Yun, and J. H. Lee, "Fabrication of a 2-D in-plane micro needle array integrated with microfluidic components using crystalline wet etching of (110) silicon," *Microsyst. Technol.*, vol. 22, no. 9, pp. 2287–2294, Sep. 2016.
- [4] X. Zhao, S. A. Coulman, S. J. Hanna, F. S. Wong, C. M. Dayan, and J. C. Birchall, "Formulation of hydrophobic peptides for skin delivery via coated microneedles," *J. Control. Release*, vol. 265, pp. 2–13, Nov. 2017.
- [5] S. Sharma, A. Saeed, C. Johnson, N. Gadegaard, and A. E. Cass, "Rapid, low cost prototyping of transdermal devices for personal healthcare monitoring," *Sens. Bio-Sensing Res.*, vol. 13, pp. 104–108, Apr. 2017.

- 1
2
3
4
5
6
7
8
9
10
11
12
13
14
15
16
17
18
19
20
21
22
23
24
25
26
27
28
29
30
31
32
33
34
35
36
37
38
39
40
41
42
43
44
45
46
47
48
49
50
51
52
53
54
55
56
57
58
59
60
61
62
63
64
65
- [6] The Organisation for Economic Cooperation and Development, "OECD Guidance document for the conduct of skin absorption studies," 2004.
 - [7] E. Hopkins and S. Sharma, *Physiology, Acid Base Balance*. StatPearls Publishing, 2019.
 - [8] N. Østergaard Knudsen and G. Pommergaard Pedersen, "pH and Drug Delivery," in *Current Problems in Dermatology (Switzerland)*, vol. 54, S. Karger AG, 2018, pp. 143–151.
 - [9] C. Surber, P. Humbert, C. Abels, and H. Maibach, "The Acid Mantle: A Myth or an Essential Part of Skin Health?," *Current Problems in Dermatology (Switzerland)*, vol. 54. S. Karger AG, pp. 1–10, 2018.
 - [10] M. R. Prausnitz *et al.*, "Skin Barrier and Transdermal Drug Delivery," in *Medical Therapy*, 2012, pp. 2065–2073.
 - [11] J. W. Fluhr and P. M. Elias, "Stratum corneum pH: Formation and function of the 'acid mantle,'" *Exogenous Dermatology*, vol. 1, no. 4. pp. 163–175, 2002.
 - [12] K. Nadendla and S. H. Friedman, "Light Control of Protein Solubility Through Isoelectric Point Modulation Corresponding Author Prof HHS Public Access," *J Am Chem Soc*, vol. 139, no. 49, pp. 17861–17869, 2017.
 - [13] S. M. Ali and G. Yosipovitch, "Skin pH: From basic science to basic skin care," *Acta Dermatovenereologica*, vol. 93, no. 3. Acta Derm Venereol, pp. 261–267, Mar-2013.